FULL AND HALF GILBERT TESSELLATIONS WITH RECTANGULAR CELLS

JAMES BURRIDGE, RICHARD COWAN, ISAAC MA

*Department of Mathematics, University of Portsmouth, Portsmouth, UK. james.burridge@gmail.com
**School of Mathematics and Statistics, University of Sydney, NSW, 2006, Australia. rcowan@usyd.edu.au
***Lee Wai Lee Vocational Studies Institute, Hong Kong. isaacma@vtu.edu.hk

Abstract. We investigate the ray–length distributions for two different rectangular versions of Gilbert's tessellation [3]. In the *full* rectangular version, lines extend either horizontally (with east- and west–growing rays) or vertically (north- and south–growing rays) from seed points which form a Poisson point process, each ray stopping when another ray is met. In the *half* rectangular version, east and south growing rays do not interact with west and north rays. For the half rectangular tessellation we compute analytically, via recursion, a series expansion for the ray–length distribution, whilst for the full rectangular version we develop an accurate simulation technique, based in part on the stopping–set theory of Zuyev [5], to accomplish the same. We demonstrate the remarkable fact that plots of the two distributions appear to be identical when the intensity of seeds in the half model is twice that in the full model. Our paper explores this coincidence mindful of the fact that, for one model, our results are from a simulation (with inherent sampling error). We go on to develop further analytic theory for the half–Gilbert model using stopping–set ideas once again, with some novel features. Using our theory, we obtain exact expressions for the first and second moment of ray length in the half–Gilbert model. For all practical purposes, these results can be applied to the full–Gilbert model — as much better approximations than those provided by Mackissack and Miles [4].

1. Introduction

Consider a stationary Poisson point process in the plane, of intensity λ. The particles of this process are called *seeds*, aptly so because at a given time $t = 0$ they each initiate the growth of a line. The directions of the lines are randomly distributed, uniformly on $(0, \pi]$, and independent of each other and of the seed locations. Each line grows bidirectionally from its seed at the same rate; thus two *rays* grow from each seed. When a ray encounters a line that has already grown across its path, the growth of that ray stops. Eventually all rays stop growth and a tessellation of the plane is formed.

The completed structure has become known as the Gilbert tessellation after Edgar N. Gilbert. It is notoriously difficult to analyse and even the expected length of a typical completed ray has not been found. There is no published paper by Gilbert on the topic; notes he supplied appear in a book by Noble, with due acknowledgement to Gilbert. Citations have typically attributed the notes to Gilbert (as we do, see [3]).

A version of the model where the directions of growth were confined to two orthogonal directions, vertical (V) and horizontal (H), was discussed by Mackissack and Miles [4]. A tessellation of the plane by rectangles results in their model. This structure too has not yielded to analysis, although when seeds are equally likely to be V or H the authors did provide an analytic approximation (based on ideas of Gilbert) to the expected ray length, namely $\sqrt{2/\lambda}$. The merits of this approximation have not been evaluated in the literature to date.

Date: January 30, 2012.

The current paper arises from work done in 1997 by the second and third authors (Cowan and Ma). They obtained some analytic results for an even simpler $V\&H$–model, whereby the growth of eastward–growing rays is halted only by southward–growing rays (and vice versa). Westward and northward have the same reciprocity. A realisation of their tessellation is given in Figure 1.

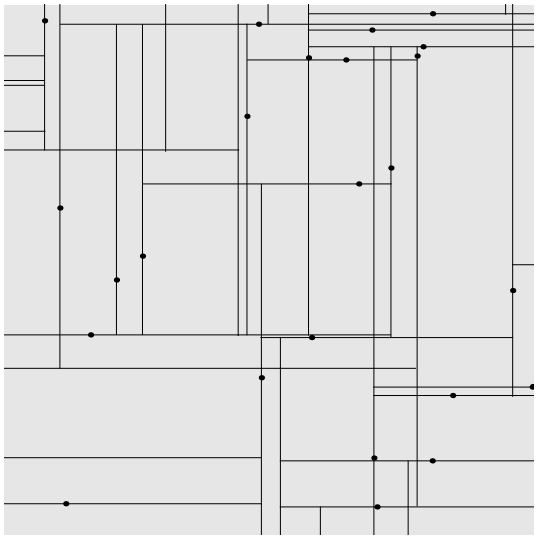

FIGURE 1. The Cowan–Ma (or half–Gilbert) rectangular tessellation when V–type and H–type seeds have equal intensities.

Cowan and Ma placed a recurrence relationship (see (1) below) from their work on the internet [2], though without proof. The background to this recurrence is as follows.

Consider the isosceles right–angle triangle POQ in Figure 2(a). Here $|OP| = |PQ| = \ell$. Suppose n seeds lie inside the triangle, uniformly and independently distributed; the figure uses $n = 6$. East or south growth of the rays is shown. Because of the blocking rules, only some of the rays reach the boundary of the triangle POQ.

Cowan and Ma investigated the probability h_n that no rays hit the boundary within the segment OP. This can also be interpreted as the probability that L, the final length of a test ray commencing eastward growth from O, is $> \ell$.

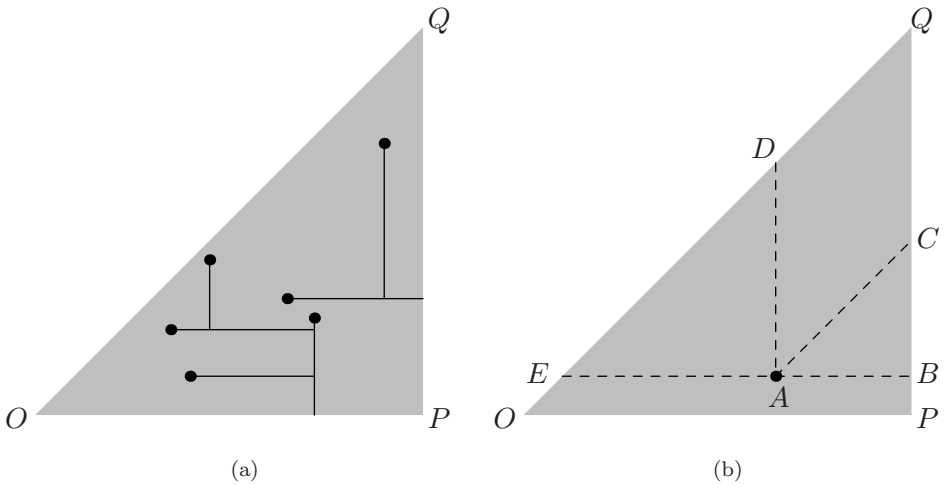

FIGURE 2. Diagrams to assist the proof of the Cowan–Ma recurrence.

Their recurrence relationship for h_n was as follows. For $n \geq 1$,

$$h_n = \frac{n!\,q}{(2n)!} \sum_{u=0}^{n-1} \sum_{v=0}^{n-1-u} \frac{2^{n-u-v}\ h_u\ h_v\ (n-1+u-v)!\ (n-1-u+v)!}{u!\ v!\ (n-1-u-v)!}, \tag{1}$$

with $h_0 = 1$. Here q is the proportion of seeds which grow horizontally. The recurrence does not involve ℓ, so h_n does not depend on ℓ — as is obvious from the scale invariance of the problem posed by Figure 2(a).

This recurrence is a useful analytic step, providing precise information on $\mathbb{E}(L)$ and $F(\ell) := \Pr\{L \leq \ell\}$.

$$F(\ell) = 1 - \sum_{n \geq 0} h_n \frac{(\lambda \ell^2)^n \exp(-\lambda \ell^2/2)}{2^n n!}, \tag{2}$$

from which we deduce (in an extended notation which includes λ) that $F_\lambda(\ell) = F_1(\sqrt{\lambda}\,\ell)$. Also

$$\begin{aligned}
\mathbb{E}(L) &= \int_0^\infty [1 - F(\ell)] d\ell \\
&= \sum_{n \geq 0} \frac{h_n}{n!} \int_0^\infty (\lambda \ell^2/2)^n \exp(-\lambda \ell^2/2) d\ell \\
&= \frac{1}{\sqrt{2\lambda}} \sum_{n \geq 0} \frac{h_n \Gamma(n + \frac{1}{2})}{n!}.
\end{aligned}$$

In Section 2, we report the proof used to derive the recurrence relationship (1) and plot the probability density function of the random variable L. The plot has an extraordinary property, discovered when certain simulations of the full rectangular–Gilbert model done by our first author, Burridge [1], were also plotted. The probability density function of the Cowan–Ma model with $\lambda = 2$ was indiscernible from that of the full rectangular–Gilbert model with $\lambda = 1$.

Section 3 presents Burridge's simulation study, that has a very high level of accuracy, and discusses this surprise coincidence — which raises somewhat the profile of the Cowan–Ma model. As well as having interest in its own right as a tessellation model with tractable mathematics, the model provides approximations for the full–Gilbert rectangular model. For example, the Cowan–Ma model — which we also called the half–Gilbert model because it has half of the blocking mechanisms — provides a much better approximation for $\mathbb{E}(L)$ in the full model when compared with the Mackissack/Miles approximation, which is $\mathbb{E}(L) \approx \sqrt{2/\lambda}$ when $q = \frac{1}{2}$.

In Section 4 our work pushes further the tractability of the half–Gilbert model finding; most notably, we find that the mean ray length when $q = \frac{1}{2}$ is given by the formula:

$$\mathbb{E}(L) = \frac{\pi}{\sqrt{\lambda}\left(\Gamma(\frac{3}{4})\right)^2}.$$

In both our simulation and analytical work we have employed Zuyev's concept of stopping set sequences [5] and the distributional results for the areas of these sets. To achieve the analytic results, we have incorporated a new concept into the analysis, the idea of dead zones which influence the formation of the next stopping set in the sequence. Our most complete analysis is for the balanced case, $q = \frac{1}{2}$, because some results become rather complicated when $q \neq \frac{1}{2}$. The expected ray length in the latter case is reported, without proof, in the appendix.

2. The Cowan–Ma recurrence relation

We now prove (1) for general q. Obviously, $h_0 = 1$ and $h_1 = \frac{1}{2}$. When $n \geq 1$, we label the seed closest to OP as A. See Figure 2(b). If the distance from A to OP is denoted by the random

variable Y, it is easily shown that Y has probability density function $g_Y(y) = 2n(1-y)^{2n-1},\ 0 \le y \le 1$. Furthermore, the conditional probability density function of $X := |AB|$ given Y is

$$g(x|y) = \frac{1}{1-y}, \qquad 0 \le x \le 1-y.$$

Denote the event that no rays hit OP by $\mathcal{E}_n$. Then

$$\begin{aligned}\Pr\{\mathcal{E}_n|x,y\} = &\ \Pr\{\text{seed } A \text{ grows eastward and reaches } B \\ &\qquad \text{and no ray grows across the segment } EA\} \\ = &\ q\Pr\{\text{no ray grows across } AB \textit{ and} \text{ no ray grows across } EA\}.\end{aligned}$$

To evaluate the right–hand side, we partition the domain above EB into the three zones that are shown in Figure 2(b). We then consider the trinomial distribution by which the remaining $(n-1)$ seeds are allocated to these zones: u to ABC, v to EAD and the remaining $(n-1-u-v)$ to $ACQD$. This leads, for each (u,v), to a rather pleasing representation of the problem into two problems self–similar to the original one. Continuing, using $||\cdot||$ as area, we write $\Pr\{\mathcal{E}_n|x,y\}$ as

$$\begin{aligned}&q\sum_{u=0}^{n-1}\sum_{v=0}^{n-1-u}\frac{(n-1)!\ ||ABC||^u\ \ ||EAD||^v\ \ ||ACQD||^{n-1-u-v}}{u!\ v!\ (n-1-u-v)!\ \ ||EBQ||^{n-1}}\ \times \\ &\qquad \Pr\{\text{no ray grows across } AB \textit{ and} \text{ no ray grows across } EA|u,v\} \\ = &\ q\sum_{u=0}^{n-1}\sum_{v=0}^{n-1-u}\frac{(n-1)!\ (\frac{x^2}{2})^u\ \ \big(\frac{(1-x-y)^2}{2}\big)^v\ \ [x(1-x-y)]^{n-1-u-v}}{u!\ v!\ (n-1-u-v)!\ \ (\frac{(1-y)^2}{2})^{n-1}}\ \times \\ &\qquad \Pr\{\text{no ray grows across } AB|u\}\Pr\{\text{no ray grows across } EA|v\} \\ = &\ q\sum_{u=0}^{n-1}\sum_{v=0}^{n-1-u}\frac{(n-1)!\ x^{2u}(1-x-y)^{2v}[2x(1-x-y)]^{n-1-u-v}}{u!\ v!\ (n-1-u-v)!\ \ (1-y)^{2(n-1)}}\ h_u\ h_v.\end{aligned}$$

Unconditional on x and y, and with $n \ge 1$,

$$\begin{aligned}h_n = &\ \Pr\{\mathcal{E}_n\} \\ = &\int_0^1\int_0^{1-y}\Pr\{\mathcal{E}|x,y\}g_Y(y)g(x|y)\ dxdy \\ = &\ q\sum_{u=0}^{n-1}\sum_{v=0}^{n-1-u}\frac{(n-1)!\ h_u\ h_v}{u!\ v!\ (n-1-u-v)!}\ \times \\ &\qquad 2n\int_0^1\int_0^{1-y}x^{2u}(1-x-y)^{2v}[2x(1-x-y)]^{n-1-u-v}\ dxdy \\ = &\ (n-1)!\ q\sum_{u=0}^{n-1}\sum_{v=0}^{n-1-u}\frac{2^{n-1-u-v}\ h_u\ h_v}{u!\ v!\ (n-1-u-v)!}\ \times \\ &\qquad 2n\int_0^1\int_0^{1-y}x^{n-1+u-v}(1-y-x)^{n-1-u+v}\ dxdy \\ = &\ n!\ q\sum_{u=0}^{n-1}\sum_{v=0}^{n-1-u}\frac{2^{n-u-v}\ h_u\ h_v}{u!\ v!\ (n-1-u-v)!}\times \\ &\qquad \int_0^1(1-y)^{2n-1}B(n+u-v,n-u+v)\ dy \\ = &\ \frac{n!\ q}{(2n)!}\sum_{u=0}^{n-1}\sum_{v=0}^{n-1-u}\frac{2^{n-u-v}\ h_u\ h_v\ (n-1+u-v)!\ (n-1-u+v)!}{u!\ v!\ (n-1-u-v)!}.\end{aligned}$$

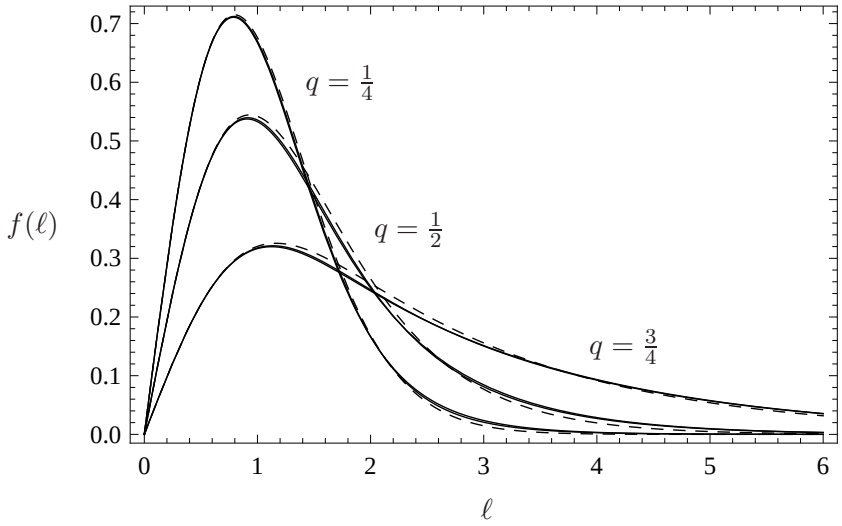

FIGURE 3. The three solid curves are the probability density functions f for the final length of a typical eastward–growing ray in the Cowan–Ma model. Each is based on $\lambda = 2$ and with three q values: $\frac{1}{4}$, $\frac{1}{2}$ and $\frac{3}{4}$. We show later in the paper that: (a) each of these solid curves actually comprises two curves overlaid, the second being the curve from the full–Gilbert model, with $\lambda = 1$; (b) the dashed lines are the probability density functions from Gilbert's heuristic 'mean field' analysis, also valid for both models.

We augment this recurrence with the result $h_0 = 1$. This completes the proof of (1). We note that the sequence $h_0, h_1, h_2, ...$ commences $1, \frac{1}{2}, \frac{1}{3}, \frac{29}{120}, \frac{11}{60}, ...$ when $q = \frac{1}{2}$.

The recurrence together with (2) can be used to plot $f(\ell) := F'(\ell)$ against ℓ for various values of q (see Figure 3).

3. Simulation of the full rectangular–Gilbert tessellation

Finding coefficients analogous to h_n for the full rectangular model is a formidable task because of the complexity of the blocking effects. Lacking self–similar zones akin to those discovered by Cowan and Ma in their model, we have devised an efficient way of accounting for these effects by simulation.

The analogue of the isosceles triangle used in Figure 2 is a square, rotated so that its diagonal AC lies east–west, as illustrated in Figure 4. To study the growth of horizontal rays, we consider an H–type *test seed* located at the western corner of the square, marked A in the figure, and define:

$$\mathbf{h}_n = \Pr\{\text{ray from test seed } A \text{ reaches } B \mid n \text{ seeds in the square}\}.$$

The only seeds that can block the test ray lie in the western side of the square, but whether or not they do so depends also on the configuration of seeds in the eastern side. Seeds outside the square have no influence.

By analogy with equation (2) the ray length distribution for the rectangular Gilbert tessellation is:

$$\mathbf{F}(\ell) = 1 - \sum_{n \geq 0} \mathbf{h}_n \frac{(2\lambda\ell^2)^n \exp(-2\lambda\ell^2)}{n!},$$

from which $\mathbf{F}_\lambda(\ell) = \mathbf{F}_1(\sqrt{2\lambda}\,\ell)$ is deduced.

An obvious method: The naive approach to estimating $\mathbf{h}_n$ would be to repeatedly populate the large square in Figure 4 with n seeds (each independently of H–type with probability q) and, each time, determine if the line AB is intersected. This can be accomplished using the following

recursive algorithm which decides if a ray, extending in compass–direction $u \in \{\rightarrow, \uparrow, \leftarrow, \downarrow\}$ from one seed s^* will be blocked within a distance d. The algorithm, block, outputs a logical value:

$$\mathsf{block}(s^*, d, u) = \begin{cases} \texttt{true} & \text{if ray is blocked} \\ \texttt{false} & \text{if ray is not blocked.} \end{cases}$$

Whether or not s^* is blocked within a distance d depends only on the configuration of seeds within a square of diagonal $2d$ along which its produced ray travels. Let the compass–direction of this ray be u, and let us denote by $\Delta(s^*, d, u)$ the isosceles triangle which forms the half of the square closest to s^*. Let the type (H or V) of seed s be $t(s)$. The algorithm $\mathsf{block}(s^*, d, u)$ runs as follows:

for all $s \in \Delta(s^*, d, u)$ **do**
  if $t(s) \neq t(s^*)$ **then**
    compute the perpendicular distance, d_s, and compass–direction, u_s from s to s^*'s produced ray.
    if $\mathsf{block}(s, d_s, u_s) =$ false **then**
      return true
    end if
  end if
end for
return false

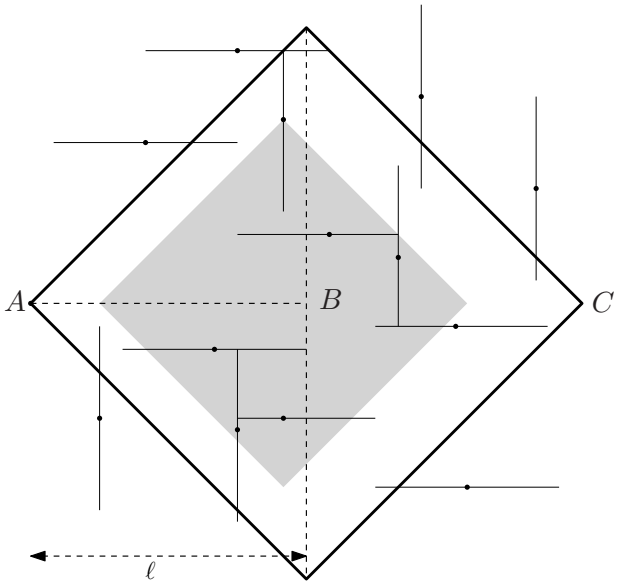

FIGURE 4. Only particles within the large square (whose diagonal is AC) can influence the event that an H–type ray starting at A does not reach B (due to intersection of the line–segment AB by vertical rays). The role of the smaller shaded square is described in the text.

For example, if s^* is the H–type seed at A, then the computer programme calls $\mathsf{block}(s^*, \ell, \rightarrow)$. This invokes recursive calls to block for every V–type seed in the left isosceles triangle (until a `true` value is returned by the call). In Figure 4, the shaded region with a V–type seed s at the top shows a square that is investigated by one of the recursive calls, specifically by the call $\mathsf{block}(s, d_s, \downarrow)$, where $2d_s$ is the diagonal length of the shaded square.

In principle, we can conduct this simulation for each n up to (say) 300. For each n, we would generate the seeds in the square (with diagonal AC) N times, where N would be very large. An estimate of $\mathbf{h}_n,\ 0 \leq n \leq 300$, is thereby generated for H–type rays. Then, if $q \neq \frac{1}{2}$, we would

repeat the whole procedure for V–type rays. It is a lengthy process, despite the potential saving if an early–tested seed s returns `true` — implying that others don't have to be tested.

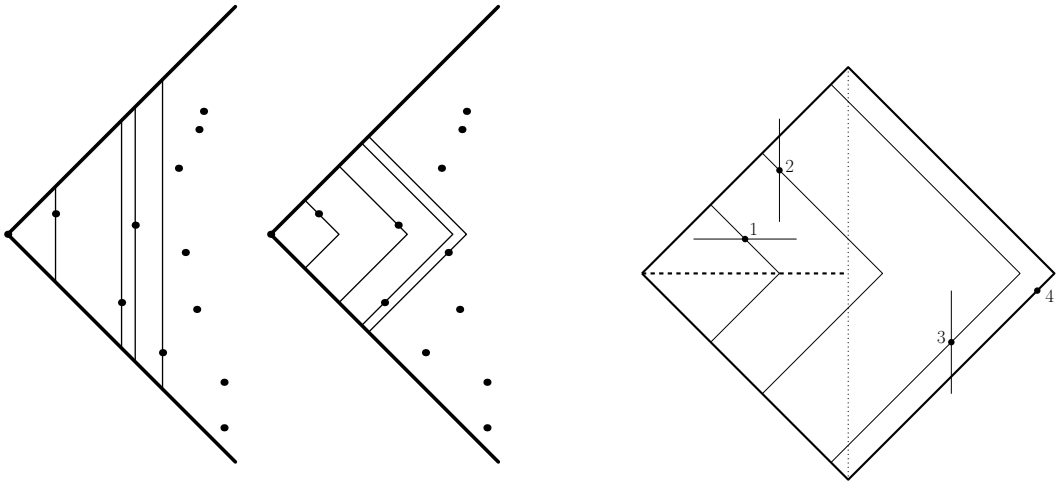

FIGURE 5. Nested stopping sets are shown in (a) and (b). In (c), the 'efficient algorithm' is at step 3 and at least one more step will be needed before we see a ray in step n crossing the dashed half–diagonal of S_{n+1}.

Stopping sets: To shorten the task, we have devised a method based on stopping sets (a concept defined by Zuyev [5] and amplified in [6]). Consider the unbounded quadrant that lies between the half–lines $y = x$ and $y = -x$, with $x \geq 0$, partly shown in Figure 5(a). A stationary Poisson process of seeds with intensity λ exists in the quadrant. A triangular set whose eastern boundary is vertical and western vertex is the quadrant's apex is gradually expanded, stopping briefly whenever its boundary hits a seed — before continuing its expansion. The set stopped by the kth seed encountered is called S_k. This process creates a nested sequence of random sets. We denote the area of S_1 by E_1 and the areas of the region $S_k \setminus S_{k-1}$ by $E_k,\ k > 1$. Another nesting arrangement is shown in Figure 5(b), this time with squares and a different ordering of the seeds.

Zuyev showed, among other things of a more general nature, that any expanding domain constructing a nest of compact sets in the manner described above — through a sequence of *stops* caused by seed hits — creates areas $E_1, E_2, E_3, ...$ which are independent and distributed exponentially with parameter λ. The domain might have a complicated geometry because the expansion rule is allowed to depend on the seeds that it contains (and, being closed, this includes seeds on the domain's boundary). In the two examples of Figure 5, the expansion rule is straightforward and doesn't depend on the internal seeds.

Most importantly for the validity of Zuyev's distributional results, neither the expansion rule nor the stopping rule for S_1 should depend on seeds *outside* the expanding domain. This prohibition plays two roles.

- it helps establish that E_1 is exponentially distributed;
- it also allows one to say that the point process of seeds outside the stopping set S_1 is still a stationary Poisson point process with unchanged intensity *given* the information within S_1 (a notion formalised by Theorem 2 of [6]).

This allows the argument to be extended sequentially to $E_2, E_3, ...$ and $S_2, S_3, ...$

We also note that Zuyev's results are not guaranteed if randomisations apart from the Poisson process of seeds affect the growth and stopping. No such complication occurs in this section of our paper, although we must address the issue later in Section 4.

Stopping sets constructed in this way have other properties. The ith seed s_i is uniformly distributed on the growth frontier of S_i and the seeds $s_1, s_2, ..., s_n$ are uniformly and independently distributed in the set S_{n+1}. Those of Figure 5(b) have a property that no other nesting has: if s_i is V–type, then whether or not it reaches the east–west diagonal depends *only* on seeds $s_1, s_2, ..., s_{i-1}$.

Efficient algorithm: In the context of Figure 5(b) with its nesting of squares, the latter property says that the ray growth just within S_{n+1} from the seeds $s_1, s_2, ..., s_n$ provides a sample of the problem that interests us — giving a *true* or *false* datum on whether a test ray is blocked before it traverses across half the diagonal of S_{n+1}. (See the illustration for $n = 3$ in Figure 5(c).) This datum contributes to the estimation of $\mathbf{h}_n$. Importantly, as we show below, if the datum is *true*, then we can add a *true* datum for the estimation of all $\mathbf{h}_j, j > n$ — without further computational effort.

We start with the unbounded quadrant empty of seeds, then place an H–type test seed at the apex of the quadrant. We generate the exponentially distributed areas E_1 and E_2 and so construct the squares S_1 and S_2 expanding from the apex. We randomly select (uniformly) a seed point s_1 on the growth frontier (eastern sides) of the inner square, S_1. Because of the properties discussed above, this is equivalent to choosing the point uniformly within the outer square S_2. If this seed grows a vertical ray that intersects the diagonal, let the distance of the intersection point from the apex be X_1. If not, set $X_1 = \infty$.

Let A_i denote $||S_i||$, the area of S_i, and $\mathcal{E}_n$ denote the event that the line from the test seed reaches the centre of a square populated with n uniformly distributed seeds. Obviously $\mathbf{h}_n = \Pr\{\mathcal{E}_n\}$.

If $X_1 < (A_2/2)^{1/2}$ then the simulation ends. There is no need to generate more nested squares in order to simulate the events $\mathcal{E}_n$, $n > 1$ because we know that the half diagonal of every subsequent square will be crossed at $X_1 < (A_n/2)^{1/2}$. Seeds on the boundaries of subsequent squares cannot influence this. If the first seed does not cross the diagonal, or crosses such that $X_1 > (A_2/2)^{1/2}$, then we draw S_3 and pick a point s_2 on the boundary of the second nested square S_2. We check if s_2 intersects the diagonal, accounting for any possible blocking effects from s_1 by using the algorithm block. If so, we let the distance from the apex to the *closest* intersection point be X_2, which will be $\leq X_1$. If $X_2 < (A_3/2)^{1/2}$ then the simulation ends. If not, we add another square S_4 and seed s_3 — reaching the situation in Figure 5(c) — and so on. We keep repeating the process — adding another seed and using block on that seed — until block indicates that the latest half–diagonal has been hit. We then record that the event $\mathcal{E}_n$ fails to occur for this and all higher values of n. The entity $\mathbf{h}_n$ for eastward growing rays is the fraction of times that $\mathcal{E}_n$ occurs over many simulations. If $q \neq \frac{1}{2}$, the complete protocol is repeated with q replaced by $(1 - q)$ to give results for southward growing rays.

To estimate the $\mathbf{h}_n$, $N = 10^9$ simulations were performed, requiring a running time of approximately one hour on a modern PC. When $q = \frac{1}{2}$, the largest number of nested squares created before the simulation terminated was 917, which occurred once, and the second largest number was 727, which also occurred once. The mean number of squares created before termination was 5.25. In the $(q = \frac{1}{2})$ case, the estimate of expected length of each line produced from a seed was:

$$\mathbb{E}(L) = 1.467535 \ (0.000029) \tag{3}$$

where the bracketed number is the standard error, calculated with due regard to the positive covariance between our estimators of $\mathbf{h}_n$ and $\mathbf{h}_{n+k}$, $k > 0$.

REMARK 1: *Our accurate estimate of the* $\mathbf{h}_n$ *values allows the probability density function of the ray length to be calculated. Because the two ray lengths coming from a particular seed are*

independent, the standard convolution method leads to an estimated distribution of the total line length arising from a typical seed. Mackisack and Miles [4] *claim that these two ray–lengths are not independent, but we disagree.*

The coincidence: We found a remarkable similarity between the probability density functions in the half rectangular Gilbert model and the full rectangular Gilbert model when the intensity of seeds in the former case was twice that of the latter case. Indeed the plots were almost indistinguishable, so Figure 3 effectively displays both f and $\mathbf{f}$ for various q, with $\lambda = 2$ or $\lambda = 1$ respectively.

We are mindful that the simulated results have sampling error, albeit small. So we asked the question: are the two distributions F and $\mathbf{F}$ mathematically equal — or just approximately so? To answer this in the $(q = \frac{1}{2})$ case, we performed some rather tedious exact calculations (details omitted) which yielded:

$$\mathbf{h}_0 = 1; \qquad \mathbf{h}_1 = \tfrac{3}{4}; \qquad \mathbf{h}_2 = \tfrac{7}{12}; \qquad \mathbf{h}_3 = \tfrac{7}{15}.$$

We then expanded both F and $\mathbf{F}$ as Taylor series about the origin.

$$\begin{aligned} F(\ell) &= h_0 + (h_1 - h_0)\ell^2 + \tfrac{1}{2}(h_0 + h_2 - 2h_1)\ell^4 \\ &\qquad + \tfrac{1}{6}(3h_1 - 3h_2 - h_0 + h_3)\ell^6 + o(\ell^7) \\ &= 1 - \tfrac{1}{2}\ell^2 + \tfrac{1}{6}\ell^4 - \tfrac{31}{720}\ell^6 + o(\ell^7). \\ \mathbf{F}(\ell) &= \mathbf{h}_0 + 2(\mathbf{h}_1 - \mathbf{h}_0)\ell^2 + 2(\mathbf{h}_0 - 4\mathbf{h}_1 + \mathbf{h}_2)\ell^4 \\ &= \qquad + \tfrac{4}{3}(3\mathbf{h}_1 - 3\mathbf{h}_2 - \mathbf{h}_0 + \mathbf{h}_3)\ell^6 + o(\ell^7) \\ &= 1 - \tfrac{1}{2}\ell^2 + \tfrac{1}{6}\ell^4 - \tfrac{32}{720}\ell^6 + o(\ell^7). \end{aligned}$$

We see that these *exact* series differ slightly in the fourth term, so F and $\mathbf{F}$ are not mathematical equal.

"Mean field" analysis when $q = \frac{1}{2}$: Gilbert's original "mean field" analysis, which was adapted by Mackisack and Miles [4] to the $(q = \frac{1}{2})$ rectangular case, involved the rough approximation that ray ends (there being two per seed) were uniformly spread across the plane. With this assumption, it was possible to approximate at time t the expected number of ray ends lying within a small distance δx of rays that would block the growth of these ends within the next δt.

Mackisack and Miles analyzed the $(q = \frac{1}{2})$ full model using two quantities; $\mathbf{R}(t)$, the expected total length of rays per unit area; $\mathbf{G}(t)$, the expected number of growing ends per unit area. Recounting their work, these quantities are related exactly by $\dot{\mathbf{R}} = \mathbf{G}$, assuming unit growth rate, and heuristically in the full rectangular case by $\dot{\mathbf{G}} \approx -\frac{1}{2}\mathbf{R}\mathbf{G}$, with initial conditions $\mathbf{R}(0) = 0$ and $\mathbf{G}(0) = 2\lambda$. Solving these differential equations, they found that $\mathbf{G}(t) \approx 2\lambda \operatorname{sech}^2\sqrt{\frac{\lambda}{2}}t$. If L is the final length of a test ray in their full Gilbert model, then:

$$\Pr(L > \ell) = \frac{\mathbf{G}(\ell)}{\mathbf{G}(0)} = \frac{\mathbf{G}(\ell)}{2\lambda} \approx \operatorname{sech}^2\sqrt{\tfrac{\lambda}{2}}t. \tag{4}$$

The expected L when $q = \frac{1}{2}$ is therefore approximated by $\sqrt{2/\lambda} = 1.41421$ at $\lambda = 1$. This is not especially close to the value shown in (3). The solution for $\mathbf{R}$ was $\mathbf{R}(t) \approx 2\sqrt{2\lambda}\tanh(\sqrt{2/\lambda}\,t)$, $t > 0$.

We have modified the analysis in [4] to deal with the $(q = \frac{1}{2})$ Cowan–Ma model. We put $\dot{G} \approx -\frac{1}{4}RG$ since each of the four directions of growing lines can only be blocked by one other line type. Solving the new equation pair, we find that the number of growing lines per unit area at time t for the half model is : $G(t) \approx 2\lambda \operatorname{sech}^2\sqrt{\frac{\lambda}{4}}t$. Also $R(t) \approx 2\sqrt{2\lambda}\tanh(\sqrt{2/\lambda}\,t)$, $t > 0$. Furthermore (4) still holds, with G replacing $\mathbf{G}$. So, setting $\lambda = 2$ in the half system and $\lambda = 1$

in the full system we obtain identical approximations to the probability density function for ray length:

$$f_2(\ell) \approx \sqrt{2}\,\mathrm{sech}^2\frac{\ell}{\sqrt{2}}\,\tanh\frac{\ell}{\sqrt{2}} \approx \mathbf{f}_1(\ell).$$

The expected ray length is: $\mathbb{E}(L) \approx \sqrt{2}$.

So we have shown that the mean field approximations in the two models are equal, when $q = \frac{1}{2}$. Indeed, our analysis for $q \neq \frac{1}{2}$, developed in the next sub–section, shows that the two approximations are also equal when $q \neq \frac{1}{2}$.

Mean field analysis when $q \neq \frac{1}{2}$: When the intensities of H- and V–type seeds are not equal, the rays of east–growing and south–growing have different length distributions. So a system of four differential equations and four initial values is needed, in variables (for the half–Gilbert model) $G_\downarrow, G_\rightarrow, R_\downarrow$ and $R_\rightarrow$.

$$\begin{aligned} \dot{R}_\rightarrow(t) &= G_\rightarrow(t) \qquad & \dot{G}_\rightarrow(t) &\approx -R_\downarrow(t)G_\rightarrow(t) \\ \dot{R}_\downarrow(t) &= G_\downarrow(t) & \dot{G}_\downarrow(t) &\approx -R_\rightarrow(t)G_\downarrow(t), \end{aligned}$$

combined with:

$$R_\rightarrow(0) = R_\downarrow(0) = 0; \qquad G_\rightarrow(0) = q\lambda; \qquad G_\downarrow(0) = (1-q)\lambda.$$

Replacing $\approx$ with $=$ and eliminating G_H and G_V, the differential equations become

$$\begin{aligned} \ddot{R}_\rightarrow(t) &= -R_\downarrow(t)\dot{R}_\rightarrow(t) \\ \ddot{R}_\downarrow(t) &= -R_\rightarrow(t)\dot{R}_\downarrow(t), \end{aligned}$$

augmented by

$$R_\rightarrow(0) = R_\downarrow(0) = 0 \qquad \dot{R}_\rightarrow(0) = q\lambda \qquad \dot{R}_\downarrow(0) = (1-q)\lambda.$$

We have only been able to solve this coupled system in series form and, even then, with no general term recognised. Using the abbreviations $Q := q\lambda$ and $P := (1-q)\lambda$,

$$\begin{aligned} R_\rightarrow(t) = \frac{Q}{1!}\,t - \frac{PQ}{3!}\,t^3 + \frac{PQ(3P+Q)}{5!}\,t^5 - \frac{PQ(15P^2+16PQ+3Q^2)}{7!}\,t^7 \\ + \frac{PQ(105P^3+241P^2Q+135PQ^2+15Q^3)}{9!}\,t^9 - ..., \end{aligned} \tag{5}$$

with $G_\rightarrow(t)$ being $\dot{R}_\rightarrow(t)$ (easily calculated from 5). A *Mathematica* routine to compute as many terms as required is available from the authors. For $R_\downarrow$ and $G_\downarrow$, simply interchange P and Q. Note that west–growing rays have results identical to east–growing — likewise north and south results are identical.

For the full–Gilbert model, the equations are very similar, but cast in terms of the four variates $\mathbf{G}_V, \mathbf{G}_H, \mathbf{R}_V$ and $\mathbf{R}_H$.

$$\begin{aligned} \dot{\mathbf{R}}_H(t) &= \mathbf{G}_H(t) \qquad & \dot{\mathbf{G}}_H(t) &\approx -\mathbf{R}_V(t)\mathbf{G}_H(t) \\ \dot{\mathbf{R}}_V(t) &= \mathbf{G}_V(t) & \dot{\mathbf{G}}_V(t) &\approx -\mathbf{R}_H(t)\mathbf{G}_V(t), \end{aligned}$$

combined with

$$\mathbf{R}_H(0) = \mathbf{R}_V(0) = 0 \qquad \mathbf{G}_H(0) = 2q\lambda \qquad \mathbf{G}_V(0) = 2(1-q)\lambda.$$

This leads to a solution for $\mathbf{R}_H(t)$ equal to the right–hand side of (5), but with $Q = 2q\lambda$ and $P = 2(1-q)\lambda$. Thus it becomes obvious that $\mathbf{R}_H(t)$ with $\lambda = 1$ equals $R_\rightarrow(t)$ with $\lambda = 2$. Likewise for the other linked pairs of variables! Therefore, when $q \neq \frac{1}{2}$, the two ray length distributions (for H and V rays) for the full model having intensity λ are equal to the corresponding ray length distributions for the half–Gilbert model with seed–intensity 2λ. All of these entities are, of course, only approximate solutions to the true Gilbert models.

Figure 3 shows that their value as approximations for the full–Gilbert model is quite good, but not nearly as good as the analytic answers adopted from the half–Gilbert model. In the last section of the paper, we provide more of these *answers*, demonstrating that the half–Gilbert model of Cowan and Ma is encouragingly tractable.

4. Stopping sets and dead zones in the half–Gilbert model.

It is possible to use the stopping–set concept to find exact expressions for the first, second and in principle higher moments of the ray length in the Cowan–Ma model. The balanced case, $q = \frac{1}{2}$, is easier to describe — and that is now our focus. We give some results for the general case in an Appendix.

A different construction of stopping sets: Suppose that a stationary Poisson process of intensity λ exists in the plane, with seeds marked either H (east growing) or V (south growing) with equal probability. In Section 3 we have described how a nest of Zuyev's stopping sets is created when the growth frontier of an expanding domain hits the seeds. For the Cowan–Ma model, the seeds that are relevant for an east–growing test ray commencing at O in Figure 2(a) is the shaded region in that figure — or, more precisely, the *unbounded* octant lying between $y = x$ and $y = 0$, with $x \geq 0$: we call this region, the initial *live zone*.

As before we start by expanding a domain — an isosceles right angle triangle in this case (see Figure 6) — into the live zone, stopping when it hits the first seed s_1 whose coordinates relative to O are (x_1, y_1). This creates a domain S_1 with area E_1 that is exponentially distributed. If s_1 is V–type, then it will provide the ray that blocks the test seed; thus $L = x_1$ and no other seeds need be considered.

Alternatively if s_1 is H–type, then, instead of growing S_1 (retaining its shape as an isosceles right–angle triangle and constructing the familiar Zuyev *nest* of stopping sets), we introduce a significant modification. We remove a part of the live zone: a 'dead zone' labelled D_1 (see Figure 6) which has now become irrelevant, as we shall soon see.

As $S_1 \cup D_1$ has been constructed without drawing upon any information taken from outside $S_1 \cup D_1$, the point process in the remaining region (the new *live zone*) is still a Poisson process with unchanged intensity given the information within $S_1 \cup D_1$ — as explained in Section 3.

We now grow a trapezium whose left–hand side located at $x = x_1$ has length $y = y_1$. The trapezium expands until its right–hand side first hits a seed s_2 (in the new live zone). The stopping set formed is called S_2. It has an exponentially distributed area E_2.

We proceed in this way, forming a sequence of stopping sets (illustrated in Figure 6) which, unlike those in Section 3, do not form a nest. They do, however, have independent exponentially–distributed areas and are part of a recursive structure which we can exploit. It is also important to note that the first V–type seed will provide the ray which blocks the test ray. Without our introduction of dead zones, a complicated algorithm rather like `block` would be required to check if a V–type ray actually reaches the path of the test ray.

Remark 2: *Why is it that no seed in D_1 can influence the distance L travelled by the test seed; dead zone V–types will either be blocked by an east–growing ray within the live zone or, if they are not blocked, the test ray must have been intersected at an earlier point. Dead zone H–types can never be in a geometrical position to block live zone V–types. The same line of reasoning applies to dead zones $D_2, D_3, ...$*

Remark 3: *In Section 3 we mentioned that extraneous randomisations, those not solely dependent on the Poisson point process, might invalidate the key results from the stopping–set theory. There is no such problem here with the stopping set S_k itself, but we note that D_k, $k \geq 1$, depends for its existence on an extraneous random feature — namely the H or V mark of seed s_k. This does not invalidate our comment above that the point process in the current live zone outside $S_k \cup D_k$ is unaffected by the information in $S_k \cup D_k$. For one thing the seed marks are independent of each other and of the point process. Furthermore, we only stop constructing dead*

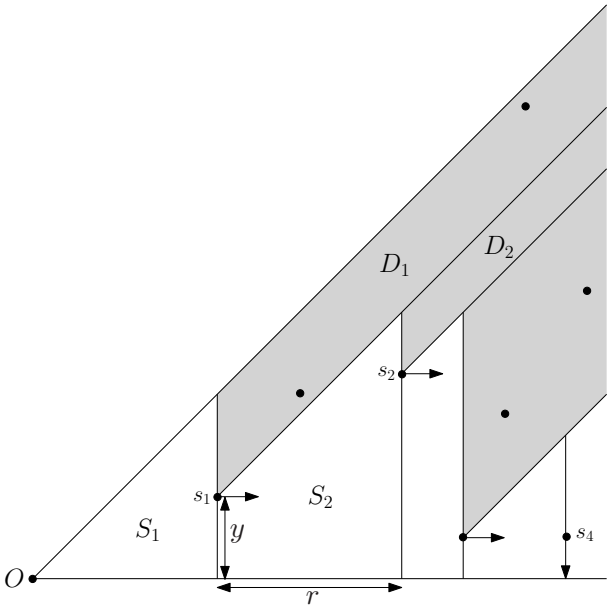

FIGURE 6. Trapezoidal stopping sets and dead zones in the half model.

zones when we have no further need to observe the process at all. So the extraneous random feature is not operative in our analysis.

The recursive structure commencing with a generic live zone: Suppose that we begin observing the process when the live zone has left boundary of height y and when we are about to construct S_n. In Figure 6, we draw the case $n = 2$. The probability density function for the length, r, of S_n's base, conditional on the height y of its left boundary, follows from the exponential distribution of S_n's area E_n. It is therefore:

$$f(r \mid y) = \lambda(r + y)e^{-\frac{\lambda}{2}(r^2+2ry)}.$$

If the stopping seed s_n for set S_n is V–type, then its south ray will be the first to intersect the test ray and the process ends. Otherwise, another dead zone is created and further trapezoidal stopping sets are formed until a V–type is met.

Let X be the random variable equal to the horizontal distance covered by stopping sets until the process comes to an end. The density function of X, conditional on y will be:

$$g(x|y) = \frac{\lambda}{2}\left[(x+y)e^{-\frac{\lambda}{2}(x^2+2xy)} + \int_0^\infty e^{-\frac{\lambda}{2}(r^2+2ry)}\left(\int_0^{r+y} g(x-r|u)du\right)dr\right], \tag{6}$$

where $g(x|y) = 0$ if $x < 0$. The first term in the square brackets accounts for the case where the first seed is V–type, and the second term for the case where it is H–type and the process is effectively re–started with a different boundary condition having already covered some horizontal distance. We have taken $q = \frac{1}{2}$, but the analysis can be carried out for general q, producing a more complicated result. Note that the ray length probability density function is $g(x \mid 0)$.

We define the moments of the conditional density:

$$\mu_n(y) = \int_0^\infty x^n g(x|y)dx.$$

As mentioned before we will here compute $\mathbb{E}(L) = \mu_1(0)$ and $\mathbb{E}(L^2) = \mu_2(0)$, which from equation (6), satisfy:

$$\mu_1(0) = \sqrt{\frac{\pi}{2\lambda}}\left[1 + \frac{\lambda}{2}\int_0^\infty \operatorname{erfc}\left(\sqrt{\frac{\lambda}{2}}u\right)\mu_1(u)du\right] \tag{7}$$

$$\mu_2(0) = \frac{2}{\lambda} + \frac{\lambda}{2}\sqrt{\frac{\pi}{2\lambda}}\int_0^\infty \operatorname{erfc}\left(\sqrt{\frac{\lambda}{2}}u\right)\mu_2(u)du + \int_0^\infty e^{-\frac{\lambda}{2}u^2}\mu_1(u)du. \tag{8}$$

Our strategy is to find $\mu_1(y)$ and $\mu_2(y)$ up to an arbitrary constant, and then to determine the constant using equations (7) and (8). The first part of this process is most easily achieved by making use of the moment generating function:

$$M_t(y) = \int_0^\infty e^{tx} g(x|y)dx,$$

which, from equation (6) satisfies

$$M_t(y) = \frac{1}{2} + \frac{1}{2}\sqrt{\frac{\pi}{2\lambda}}e^{\frac{(\lambda y - t)^2}{2\lambda}}\left\{\operatorname{erfc}\left(\frac{\lambda y - t}{\sqrt{2\lambda}}\right)\left[t + \lambda\int_0^y M_t(u)du\right] + \lambda\int_y^\infty \operatorname{erfc}\left(\frac{\lambda u - t}{\sqrt{2\lambda}}\right)M_t(u)du\right\}.$$

This integral equation may be reduced to the differential equation:

$$\frac{d^2M_t}{dy^2} - (\lambda y - t)\frac{dM_t}{dy} - \frac{\lambda}{2}M_t = -\frac{\lambda}{2}.$$

Expressing the left hand side as a series in t, and collecting coefficients of t and t^2 we obtain differential equations satisfied by $\mu_1(y)$ and $\mu_2(y)$:

$$\mu_1''(y) - \lambda y\mu_1'(y) - \frac{\lambda}{2}\mu_1(y) = 0 \tag{9}$$

$$\mu_2''(y) - \lambda y\mu_2'(y) - \frac{\lambda}{2}\mu_2(y) = -2\mu_1'(y). \tag{10}$$

Clearly we must solve for $\mu_1(y)$ first.

The first conditional moment: Making the change of variable $z = (\frac{\lambda}{2})^{\frac{1}{2}}y$ in equation (9) we obtain:

$$\frac{d^2\mu_1}{dz^2} - 2z\frac{d\mu_1}{dz} - \mu_1 = 0.$$

If the coefficient of μ_1 were a positive multiple of two, this would be Hermite's equation, solved by Hermite polynomials. Since this is not the case, we seek a series solution [7]:

$$\mu_1(y(z)) = \sum_{n=0}^\infty a_n z^n$$

and obtain the recurrence relation:

$$a_{n+2} = \frac{2n+1}{(n+1)(n+2)}a_n.$$

This leads to the general solution:

$$\mu_1(y(z)) = a_0 M(\tfrac{1}{4}, \tfrac{1}{2}, z^2) + a_1 z\ M(\tfrac{3}{4}, \tfrac{3}{2}, z^2),$$

where M is Kummer's Function [8]:

$$M(a, b, z) = \sum_{n=0}^\infty \frac{(a)_n z^n}{(b)_n n!}.$$

Here we have used the Pochhammer symbol, defined by:

$$(a)_n = a(a+1)(a+2)...(a+n-1),\ (a)_0 = 1.$$

The Kummer's functions diverge as $z \to \infty$, but we know that $\mu_1(y(z)) \to 0$ in that limit. This apparent paradox is resolved by noting that the two independent parts of the solution may be combined to form a Kummer's function of the second kind [8], defined by:

$$U(a,b,z) = \frac{\pi}{\sin \pi b}\left[\frac{M(a,b,z)}{\Gamma(1+a-b)\Gamma(b)} - z^{1-b}\frac{M(1+a-b,2-b,z)}{\Gamma(a)\Gamma(2-b)}\right]$$

which tends to zero as $z \to \infty$. In terms of this function, the general solution is:

$$\mu_1(y(z)) = A \times M(\tfrac{1}{4},\tfrac{1}{2},z^2) + B \times U(\tfrac{1}{4},\tfrac{1}{2},z^2).$$

It must be the case that $A = 0$ in order to capture the right asymptotic behavior so, restoring the original variable y, the conditional moment must have the form:

$$\mu_1(y) = B \times U(\tfrac{1}{4},\tfrac{1}{2},\tfrac{\lambda}{2}y^2). \tag{11}$$

It now remains to compute B. We do this by substituting (11) into equation (7). Making use of the result:

$$\int_0^\infty \mathrm{erfc}(u)U(\tfrac{1}{4},\tfrac{1}{2},u^2)du = \frac{\sqrt{2}}{\pi}[\Gamma(\tfrac{1}{4}) - \sqrt{\pi}\Gamma(\tfrac{3}{4})],$$

together with $\Gamma(\frac{1}{4})\Gamma(\frac{3}{4}) = \sqrt{2}\pi$ we find that:

$$B = \frac{\sqrt{\pi}}{\sqrt{\lambda}\Gamma(\frac{3}{4})}.$$

We have now found $\mu_1(y)$, which gives us a compact analytic expression for the expected ray length:

$$\begin{aligned}\mathbb{E}(L) &= \mu_1(0)\\ &= \frac{\sqrt{\pi}}{\sqrt{\lambda}\Gamma(\frac{3}{4})}U(\tfrac{1}{4},\tfrac{1}{2},0)\\ &= \frac{\pi}{\sqrt{\lambda}\left(\Gamma(\frac{3}{4})\right)^2}\\ &\approx \frac{2.0920992}{\sqrt{\lambda}}\end{aligned}$$

For comparison, using the first 200 coefficients from Cowan and Ma's recurrence we obtain $\mathbb{E}(L) \approx 2.0920987$ when $\lambda = 1$. As we discovered earlier, when $\lambda = 2$, the half model provides an approximation to the full model, having similar but simplified blocking effects and identical mean field behaviour. For this choice of λ we obtain the exact half model result $\mathbb{E}(L) = 1.479337560$ to 7 decimal places, which differs from the accurate full model result (1.467535) by 0.7%. Compared with the mean field prediction: $\mathbb{E}(L) \approx \sqrt{2}$, which differs from the full model by 3.6% this is a much closer approximation.

The second conditional moment: As for the calculation of μ_1, we make the change of variable $z = (\frac{\lambda}{2})^{\frac{1}{2}}y$, but this time in equation (10), obtaining

$$\frac{d^2\mu_1}{dz^2} - 2z\frac{d\mu_1}{dz} - \mu_1 = \frac{\sqrt{2\pi}z}{\lambda\Gamma(\frac{3}{4})}U(\tfrac{5}{4},\tfrac{3}{2},z^2),$$

where we have used the differential property [8] : $U'(a,b,z) = -a\ U(a+1,b+1,z)$. We know the homogeneous part of the general solution to (10), so it remains to find a particular solution.

We do this using variation of parameters, and begin by making the definitions:

$$f_1(z) = M(\tfrac{1}{4}, \tfrac{1}{2}, z^2)$$
$$f_2(z) = U(\tfrac{1}{4}, \tfrac{1}{2}, z^2).$$

The function M has the differential property [8]: $M'(a, b, z) = \frac{a}{b} M(a + 1, b + 1, z)$ which allows us to compute the Wronskian:

$$\begin{aligned} W(z) &= f_1(z) f_2'(z) - f_2(z) f_1'(z) \\ &= -\frac{z}{2} \left[M(\tfrac{1}{4}, \tfrac{1}{2}, z^2) U(\tfrac{5}{4}, \tfrac{3}{2}, z^2) + 2U(\tfrac{1}{4}, \tfrac{1}{2}, z^2) M(\tfrac{5}{4}, \tfrac{3}{2}, z^2) \right]. \end{aligned}$$

We now define

$$G(z, t) = \frac{f_2(z) f_1(t) - f_1(z) f_2(t)}{W(t)}$$

in terms of which the particular integral is:

$$f_p(z) = -\frac{\sqrt{2\pi}}{\lambda \Gamma(\frac{3}{4})} \int_z^\infty G(z, t) t U(\tfrac{5}{4}, \tfrac{3}{2}, t^2) dt.$$

Discarding the divergent part of the solution, and restoring y, we have that:

$$\mu_2(y) = C \times U(\tfrac{1}{4}, \tfrac{1}{2}, \tfrac{\lambda}{2} y^2) - \frac{\sqrt{2\pi}}{\lambda \Gamma(\frac{3}{4})} \int_{z(y)}^\infty G(z(y), t) t U(\tfrac{5}{4}, \tfrac{3}{2}, t^2) dt,$$

where C is an as yet undetermined constant. We find it by substituting our expression for $\mu_2(y)$ into equation (8). Making use of the numerical integral:

$$\begin{aligned} K &= -\int_0^\infty \operatorname{erfc}(z) \left[\int_z^\infty G(z, t) t U(\tfrac{5}{4}, \tfrac{3}{2}, t^2) dt \right] dz \\ &= 0.343146 \end{aligned}$$

we find that:

$$C = \frac{1}{\Gamma\left(\frac{3}{4}\right) \lambda} \left(\frac{\pi K}{\Gamma\left(\frac{3}{4}\right)} + 2\sqrt{2} \right).$$

Noting also that $f_p(0) = \frac{2}{\lambda}$ we have the final result that:

$$\begin{aligned} \mathbb{E}(L^2) &= \mu_2(0) \\ &= \frac{1}{\Gamma\left(\frac{3}{4}\right) \lambda} \left(\frac{\pi K}{\Gamma\left(\frac{3}{4}\right)} + 2\sqrt{2} \right) U(\tfrac{1}{4}, \tfrac{1}{2}, 0) + f_p(0) \\ &= \frac{\pi^{3/2} K + 2\Gamma\left(\frac{3}{4}\right) \left(\sqrt{2\pi} + \Gamma\left(\frac{3}{4}\right)^2 \right)}{\lambda \Gamma\left(\frac{3}{4}\right)^3} \\ &\approx \frac{6.37688}{\lambda} \end{aligned}$$

For comparison, using the first 200 coefficients from the Cowan–Ma recurrence we obtain $\mathbb{E}(L) \approx 6.37686$ when $\lambda = 1$.

5. Concluding comment

Gilbert's tessellation is notoriously difficult to analyse, and even the rectangular version studied by Mackisack and Miles remains entirely without analytical results. In this paper we have shown that the simplified rectangular model of Cowan and Ma, with only half of the blocking rules of the Mackisack and Miles model, has a number of tractable properties. As such, it is the only Gilbert–style model, we believe, which has yielded any analytic results.

Appendix: Expected length in the half model when $q \neq \frac{1}{2}$

If q is the proportion of seeds growing horizontally in the half model, then equation (6) becomes:

$$g(x|y) = (1-q)\lambda(x+y)e^{-\frac{\lambda}{2}(x^2+2xy)} + q\lambda \int_0^\infty e^{-\frac{\lambda}{2}(r^2+2ry)} \left[\int_0^{r+y} g(x-r|u)du \right] dr.$$

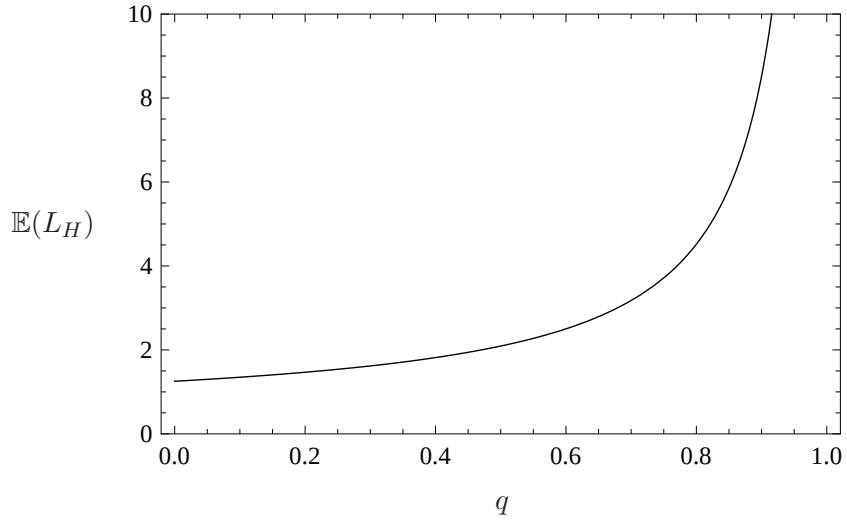

FIGURE 7. Expected horizontal length in the half model as a function of q, the proportion of horizontal rays. The seed density is $\lambda = 1$.

The first moment of $g(x|0)$ may be found by similar methods to those employed in the $q = \frac{1}{2}$ case. The expected length of a horizontal ray is found to be:

$$\mathbb{E}(L_H) = \sqrt{\frac{\pi}{\lambda}} \left[\sqrt{2} - \frac{q\Gamma\left(1-\frac{q}{2}\right) G^{2,3}_{3,3}\left(1 \left| \begin{matrix} 0, \frac{1}{2}, \frac{q+1}{2} \\ 0, \frac{1}{2}, -\frac{1}{2} \end{matrix} \right.\right)}{2^{q+\frac{1}{2}}\pi\Gamma(1-q)} \right]^{-1}$$

where G is Meijer's G–Function [9]. Figure 7 illustrates the function $\mathbb{E}[L_H]$ for the case $\lambda = 1$.

References

[1] Burridge, J. (2010). *Simulation of the rectangular Gilbert tessellation.* Unpublished Technical Report.

[2] Cowan, R. and Ma, I.S.W. (2002). Solving a simplified version of the Gilbert tessellation. On the website *www.maths.usyd.edu.au/u/richardc/unsolved.html*

[3] Gilbert, E. N. (1967) Surface Films of Needle–Shaped Crystals, In *Applications of Undergraduate Mathematics in Engineering*, B. Noble (editor), Macmillan, pp. 329–346.

[4] Mackisack, M. S. and Miles, R. E. (1996). Homogeneous Rectangular Tessellations. *Adv. Appl. Prob.* **28** 993.

[5] Zuyev, S. (1999). Stopping Sets: Gamma–type results and hitting properties. *Adv. Appl. Prob.* **31** 355–366.

[6] Cowan, R., Quine, M. and Zuyev, S. (2003). Decomposition of Gamma–distributed domains costructed from Poisson Point Processes. *Adv. Appl. Prob.* **35** 56–69.

[7] Mathews, J. and Walker R. L. (1973). *Mathematical Methods of Physics.* Addison Wesley.

[8] Abramowitz, M. and Stegun, A. (1970). *Handbook of Mathematical Functions.* Dover Publications, New York.

[9] Gradshteyn, I.S. and Ryzhik, I.M. (2007). *Table of Integrals, Series, and Products.* Seventh Edition. Academic Press.